11A.5 Validation of attenuation correction at X band performed with collocated S-band polarimetric radar

V. Melnikov[*], D. Zrnic[+], A. Ryzhkov[*], A. Zahrai[+], and J. Carter[*]

[*]*Cooperative Institute for Mesoscale Meteorological Studies, Oklahoma University,*
[+]*NOAA/OAR National Severe Storms Laboratory, Norman OK.*

1. Introduction

X-band weather radars have several advantages in comparisons with C- and S-band radars: a smaller antenna for the same bandwidth, smaller hardware for the same sensitivity, lower power consumption and cost. These allows building compact mobile radars for various field experiments (e.g., Anagnostou et al., 2004, Alexander and Wurman, 2005; Park et al., 2005, Pazmany et al. 2003, Blustein et al., 2007; Yanjiao et al, 2008). Dual polarization capability becomes a standard for weather radars because it allows obtaining important information on scattering media and improving rain rate retrievals. Polarimetric X-band radar has one more important advantage: the specific differential phase, K_{dp}, is much larger than ones at C and S bands. This allows accurate measurements of K_{dp} even in light rain. K_{dp} does not depend on radar calibration; it is less sensitive to variations in precipitation parameters and relatively immune to attenuation.

X-band radiation experiences attenuation in even light precipitation so measured reflectivity Z and differential reflectivity Z_{DR} must be corrected for attenuation. At ranges longer than 50 km, attenuation in oxygen, water vapor and clouds should be taken into consideration. Rain rate R obtained from K_{dp} is more accurate than the conventional Z-R relation, but it is more "noisy" due to fluctuations in the differential phase and It experiences also influence of the differential phase upon scattering δ.

Attenuation correction at X band is done using two approaches. The first is based on a nearly linear fit between attenuation and the differential phase (Chandrasekar and Bringi, 2001). This approach was successfully used at X band within 50 km from radar and reflectivities less than about 40 dBZ (e.g., Matrosov et al. 2006, Yanjiao et al. 2008). For stronger reflectivities and longer distances, self-consistent procedures are usually utilized (Park et al. 2005, Anagnostou et al. 2006).

Valery.Melnikov@noaa.gov

In this paper, we apply the latter approach to correct reflectivities and differential reflectivities at X band and compare the results with data collected with a collocated S-band polarimetric radar. Range of our observations is 150 km and reflectivities reach 70 dB at S band.

2. XERES' parameters

The Oklahoma University and NSSL have designed mobile X-band dual-polarization radar called XERES, i.e., X-band Experimental Radar for the Examination of Storms (Fig.1). XERES employs a polarization configuration with **S**imultaneous transmittion and reception of **H**orizontally and **V**ertically polarized waves (**SHV** scheme). The main radar parameters are listed in Table 1 along with ones of WSR-88D KOUN. Antenna patterns in the horizontal plane are depicted in Fig. 2.

Table 1. Parameters of XERES and WSR-88D KOUN

Parameter	**XERES**	**WSR-88D KOUN**
Wavelength (cm)	3.2	11.1
Frequency, MHz	9410	2705
Pulse power at antenna (kW), each channel	50	160
Pulse width (us)	0.25; 0.5; 1.0; 2.0	1.54; 4.5
Transmitter tube	Magnetron	Klystron
Antenna type & size (m)	Circular paraboloid, 2.5	Circular paraboloid, 8.54
3-dB antenna beamwidth, (deg.)	0.90 (Hor) 0.95 (Vert)	0.95 (Hor) 0.94 (Vert)

Parameter	**XERES**	**WSR_88D KOUN**
Antenna gain, dB	45	44.5
First copolar sidelobe, dB	-22.5 @1.33^o	-31@1.0^o
Antenna struts (number and angles)	3 (0^o, -120^o, +120^o)	3 (0^o, -120^o, +120^o)
Radom, diameter, m	N/A	11.9
Minimum detectable signal (dBm)	-112	-114
Receiver dynamic range, dB	90	95

Parameter	**XERES**	**WSR_88D KOUN**
Unambiguous velocity (m s^{-1})	4 … 32	27… 35
Polarization scheme	SHV	SHV
Measurable parameters	Z, v, σ_v, Z_{DR}, ρ_{hv}, φ_{dp}	Z, v, σ_v, Z_{DR}, ρ_{hv}, φ_{dp}
Number of range gates	1000	1200
Radial resolution (m)	37, 75, 150, 300	250, 750

Fig. 1. XERES mobile radar: (left) the antenna, (right) the radar deployed near the WSR-88D KOUN for the experiment.

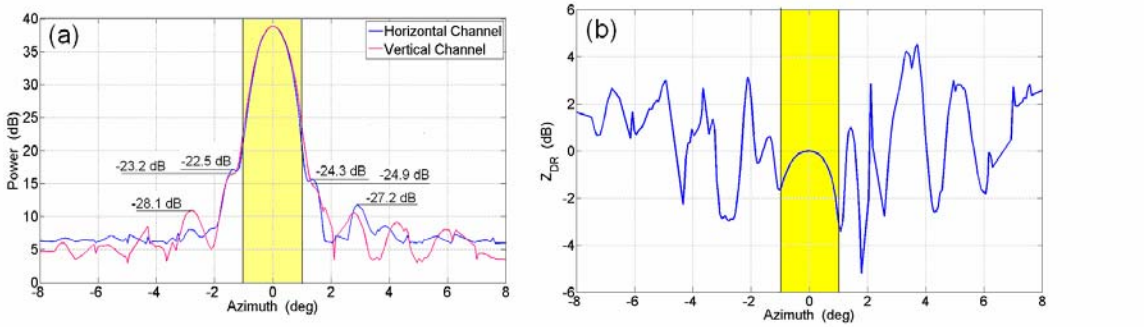

Fig. 2. Antenna patterns in the horizontal plane: (a) one-way power diagram and (b) differential reflectivity. Area of -1^o to +1^o is highlighted yellow.

3. Experimental setup and radar data

In fall 2008 and spring 2009 XERES was deployed near the dual-polarization S-band WSR-88D KOUN situated in central Oklahoma. Both radars have a 1 deg beamwidth and employ same polarization technique with simultaneous transmission and reception of horizontally and vertically polarized waves. The radars executed Volume Coverage Patterns (VCP) with the same elevations. XERES' VCP were 190-degree sector scans whereas KOUN executed 360-degree slant scans so that the VCPs were not fully synchronized in time. An example of reflectivity and differential reflectivity fields collected with the two radars is presented in Fig. 3. Radar data from same elevations with time difference less than 20 seconds has been taken for our analysis that allowed nearly radial-by-radial comparisons of radar variables. Radial resolution on KOUN was 250 m and the vast majority of XERES' data was collected with radial resolution of 150m. The range of data collection with XERES was 150 km (PRF = 1000 Hz); KOUN collected data up to 300 km but herein we present KOUN's data within 150 km for easy comparisons with XERES' data.

KOUN collected data at elevations 0.5°, 1.45°, 2.5°, 3.5°, .. spaced by about 1° at low elevations. XERES' collected data at the same elevations. We analyzed data collected at elevations 1.45° and upper, X-band data at elevation of 0.5 ° were frequently blocked by nearby targets. Radar data were collected from clouds, stratiform rain, and tornadic thunderstorms. Reflectivity difference at the two wavelengths before attenuation correction can reach 40 dBZ which is a result of attenuation at X-band and resonant effects. The latter we discuss in section 5. Due to differential attenuation, differential reflectivity at X-band can drop below -5 dB and the difference in Z_{DR} at two wavelengths exceeded 6 dB.

4. Attenuation correction at X band

We assume that radar reflectivity Z is measured at horizontal polarization and we will omit an additional subscript referring to that. Attenuation of radiation is a primary source of errors at X band. There are three main contributors to attenuation – atmospheric gases, cloud water, and precipitation. The later is usually stronger than the rest ones thus the main attention is paid to corrections for attenuation in rain especially at distances within 50 km. At longer distances, attenuation by gases should be taken into consideration. This attenuation is a result of absorption by water vapor and oxygen (Ulabi et al. 1981, section 5).

Attenuation by cloud water is difficult to asses because the water content varies in large interval and it does not contribute to return radar signal at X band due to small sizes of water cloud droplets. We analyze herein radar data collected at low elevations and omit this contribution to attenuation.

To correct Z and Z_{DR} for attenuation at X-band, two main methods are usually applied – the linear fit approach (e.g., Bringi et al. 1990, Matrosov et al. 2005, Yanjiao et al. 2008) and the self-consistent methods with constraints (Hitchfield and Bordan 1954, Marzoug and Amayenc 1991, Testud et al. 2000, Park et al. 2005, Anagnostou et al. 2006). The linear fit method relates the attenuated parts of reflectivity ΔZ and differential reflectivity ΔZ_{DR} to the differential phase φ_{dp} as follows

$$\Delta Z = f_1 \varphi_{dp}, \quad (1)$$

$$\Delta Z_{DR} = f_2 \varphi_{dp}, \quad (2)$$

with constants f_1 and f_2. The latter for X and S bands listed in Table 2. This method works well in weak to moderate precipitation with reflectivities less than 38 dBZ and distances less than 50 km (Matrosov et al. 2005, 2006).

Table 2. Coefficients f_1 and f_2 in relations (1) and (2)

	X band	S band
f_1	0.25	0.04
f_2	0.033	0.004

The self-consistent method relates measured $Z_m(r)$ and $Z_{DRm}(r)$ at distance r to the intrinsic $Z(r)$ and $Z_{DR}(r)$ using φ_{dp} constraints. The measured and intrinsic variables are related as

$$Z_m(r) = Z(r)\exp\left[-0.2\ \ln(10)\int_{r_1}^{r} A(r)dr\right], \quad (3)$$

$$Z_{DRm}(r) = Z_{DR}(r) - 2\int_{r_1}^{r} A_{dp}(r)dr), \quad (4)$$

where A and A_{dp} are attenuation at horizontal polarization and differential attenuation at H- and V-polarizations expressed in dB/km, Z_{DR} is in dB, Z in is in $mm^6\ m^{-3}$, the radar echo is located between ranges r_1 and r_2, and $r_1 \le r \le r_2$.

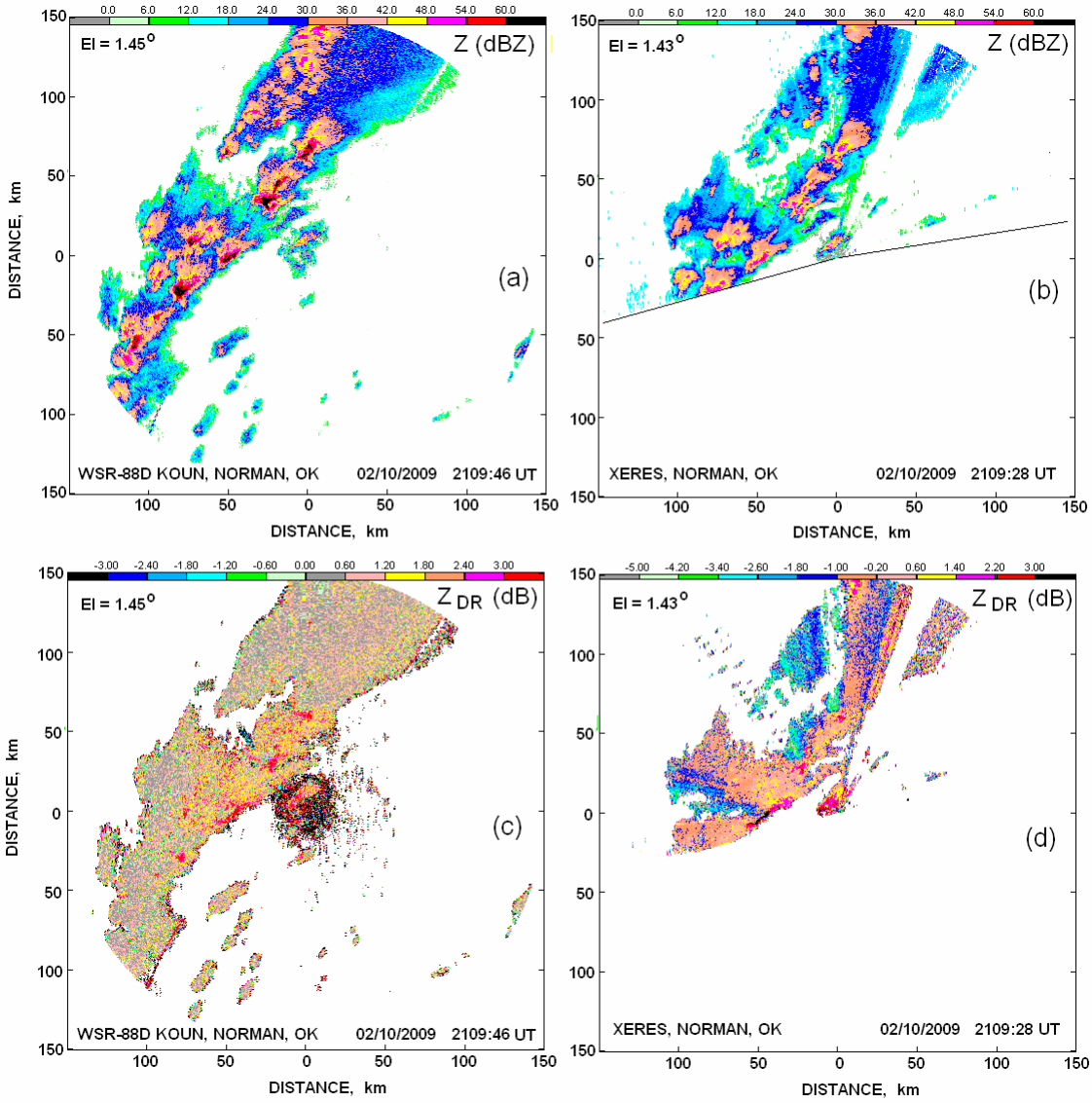

Fig. 3. Examples of PPI scans of measured reflectivities with KOUN (a) and XERES (b) on February 10, 2009. Differential reflectivities are shown in panels (c) and (d). Data display on KOUN is restricted at range of 150 km for easy comparisons. The sector of data collection with XERES is shown with two thin black lines. No attenuation correction is applied to XERES' data.

Using the following empirical relations between A, Z, and specific attenuation K_{dp}:

$$A = aZ^b, \quad (5)$$

$$A = \alpha K_{dp}^c, \quad (6)$$

$$A_{dp} = \gamma A^d, \quad (7)$$

attenuation A is obtained with a constraint that total attenuation at the far end of a radar echo is consistent with the total change of differential propagation phase Φ_{dp}:

$$A(r) = \frac{Z_m^b(r)B}{I(r_1, r_2) + I(r, r_2)B}, \quad (8)$$

$$I(r, r_2) = 0.46b\int_r^{r_2} Z_m^b(r)dr,$$

$$B = \exp[0.1\alpha b \ln(10)\Phi_{dp}] - 1.$$

Exponent c in (6) is close to one. It is seen from (3) and (4) that measured reflectivity and differential reflectivity depend on integral of attenuation. Integrating (8) we get

$$\int_{r_1}^{r} A(r)dr = \frac{1}{0.46b}\ln\frac{B+1}{B\ \Delta I(r)+1}, \qquad (9)$$

$$\Delta I(r) = \frac{I(r,r_2)}{I(r_1,r_2)}.$$

For c = 1 in (6), corrected reflectivity in dBZ is obtained by substituting (9) into (3):

$$Z(r) = Z_m(r) + \alpha\Phi_{dp} - 10b^{-1}\log_{10}[1+\Delta I(r)B] \ \text{(dBZ)}, \qquad (10)$$

Coefficient α in (6) depends on the drop size distribution, drop shapes, and temperature; it varies in interval 0.139 to 0.335. To mitigate these variations, an additional constraint was used to minimize error difference $\Delta\varphi_{dp}$ between the measured&filtered differential phase profile and calculated one via (Park et al. 2005)

$$\Delta\varphi_{dp}(\alpha) = \left|\ \varphi_{dp}(r) - \frac{2}{\alpha}\int_{r_1}^{r} A(\alpha,r)dr\ \right|. \qquad (11)$$

Considering (11) for the whole distance, we write

$$\Delta\varphi_{dp}(\alpha) = \int_{r_1}^{r_2} \left|\ \varphi_{dp}(r) - \frac{2}{\alpha}\int_{r_1}^{r} A(\alpha,r)dr\ \right| dr. \qquad (12)$$

Using (9) the latter is written as

$$\Delta\varphi_{dp}(\alpha) = \int_{r_1}^{r_2} \left|\ \Phi_{dp} - \varphi_{dp}(r) - 10\alpha^{-1}b^{-1}\log_{10}[1+\Delta I(r)B]\ \right| dr. \qquad (13)$$

Once α is obtained, $Z(r)$ is calculated via (10). Corrected differential reflectivity for d = 1 in (7) is calculated as:

$$Z_{DR}(r) = Z_{DRm}(r) + \gamma\alpha\Phi_{dp} - 10\gamma b^{-1}\log_{10}[1+\Delta I(r)B]\} \ \text{(dB)}. \qquad (14)$$

The empirical coefficients that enter in relations (5)-(7) at X band are listed in Table 3.

Table 3. Coefficients in empirical relations (5)-(7) at X band

	Minimal value	Maximal value
a	$9.781\ 10^{-5}$	$1.749\ 10^{-4}$
b	0.757	0.804
α	0.139	0.335
c	1.00	1.312
γ	0.114	0.174
d	1.042	1.239

There is a difficulty in application of the above method for strong reflectivity cases: the backscatter differential phase affects obtaining the propagation part of the differential phase. The measured differential phase ψ consists of two parts: the propagation contribution φ_{dp} and the backscatter phase δ: $\psi = \varphi_{dp} + \delta$. In precipitation with reflectivities lower than 40 dBZ, δ is small and can be neglected, thus $\psi = \varphi_{dp}$. At stronger reflectivities, δ must be eliminated in order to obtain the propagation part of differential phase and relate it to attenuation. Fig. 4 illustrates the issue. It is seen that the measured phase ψ has a strong positive spike at ranges 54 to 60 km which is a manifestation of a strong δ. Hubbert and Bringi (1993) proposed an iterative FIR filter to eliminate δ. We used a filter based on identification of positive δ–humps. Examples of ψ and φ_{dp} profiles are shown in Fig. 9(b,c,d).

In Fig. 5, typical range profiles of Z and Z_{DR} are shown wherein reflectivities are lower than 45 dBZ. One can see that the correction procedures work well. If reflectivities exceed 45 dBZ at S-band, we see underestimation of attenuation as in Fig. 6(a,c). Such underestimation could result from inherent assumptions of the method, i.e., a and b in (5) are constant and c =1 in (6) at strong Z. Scattering simulations show that at Z larger than 45 dBZ, relations (5)-(7) are not stable, i.e., the scatterplots of the parameters are wide. Another source of errors could be due to the presence of ice graupel. If ice particles are spherical in the mean, then they do not contribute to the differential phase but their contribution in attenuation can be significant. This attenuation can be strong in cases of wet or spongy graupel.

In some cases, we noticed overestimation of corrected Z and Z_{DR} as in Fig. 6(b,d) that resulted from overestimation of attenuation. This occurs when Z-profile at X band ends up at S band Z about 40 dBZ and higher. Such reflectivities could have a significant δ at X band that cannot be eliminated. Thus measured differential phase ψ is totally attributed to φ_{dp} which leads to its overestimation due to a contribution from δ.

Underestimation of attenuation (Figs 5 a,c) occurs more frequently than overestimation (Figs. 5b,d).

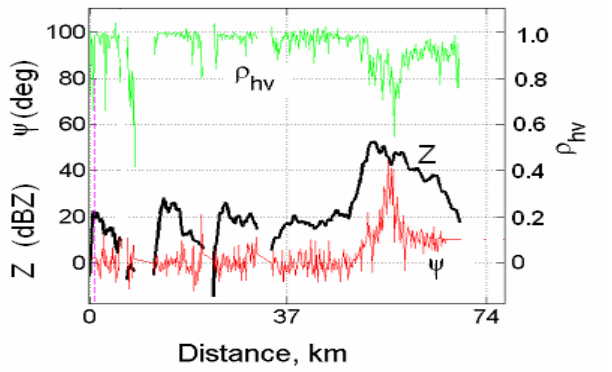

Fig. 4. Range profile of X-band reflectivity Z, phase ψ, and correlation coefficient ρ_{hv} at Az= 356.5° El=3.45° on 10 February 2009 at 205955 UTC.

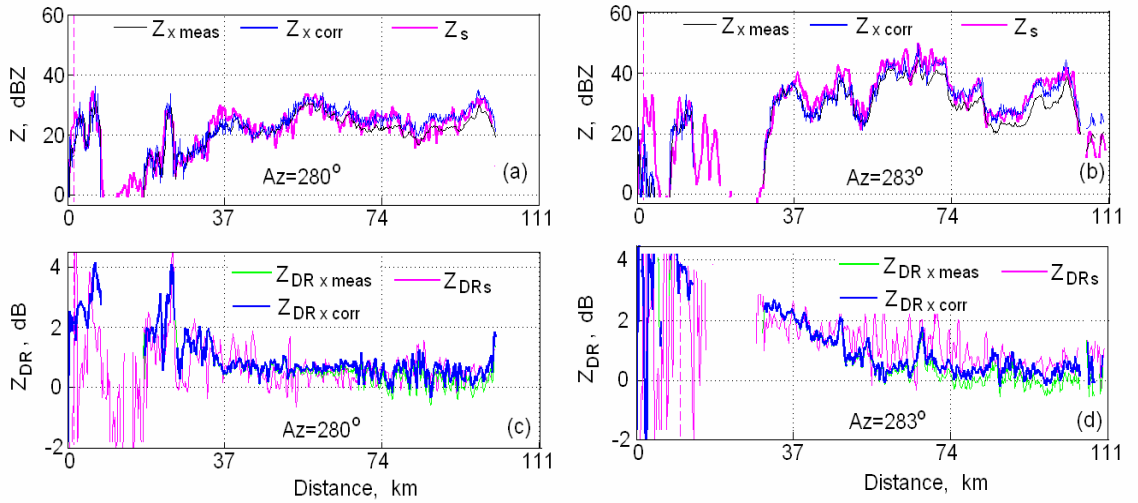

Fig. 5. (a, b): Range profiles of reflectivities at X and S bands and (c, d) differential reflectivities.10 February 2009.

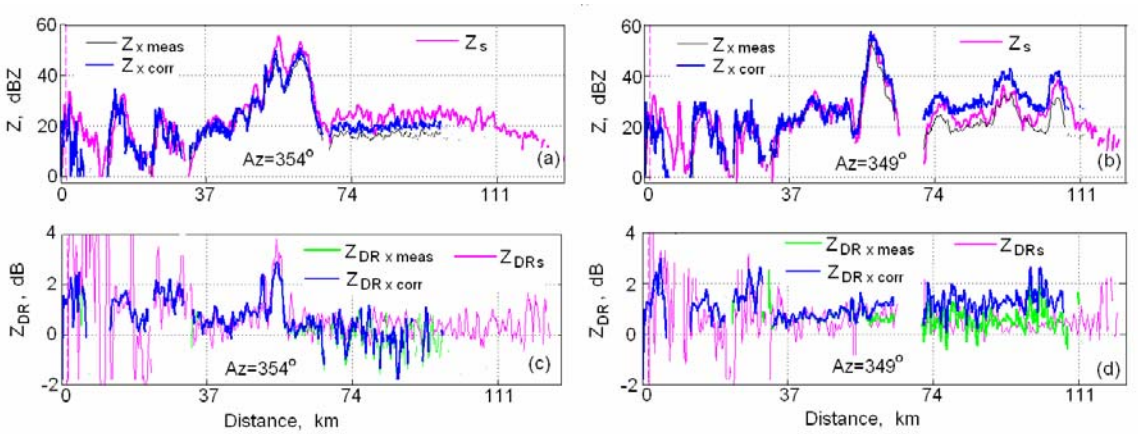

Fig. 6. Same as in Fig. 5 but for different azimuths.

5. Hail

Thunderstorms on February 10, 2009 produced hail. S-band reflectivities reached 70 dBZ. The supercell in azimuth near 250 at distance about 80 km (Fig. 3) produced tornadoes. There were numerous reports on hail on the ground during this event.

In the presence of hail, reflectivities at S and X bands can differ significantly which is well known. Fig. 7 illustrates reflectivity difference for a single scatterer. The blue line is for water drops; the line continues to size of 15 mm for cases of a graupel covered by a water film. For very large water particles, the aspect ratio was calculated according to Brandes et al. (2002). The red line is for an ice sphere. It is seen that reflectivities at S band can exceed the ones at X band by several dB for scatterers with diameters of 10-14 mm. So in the presence of hail, reflectivities at S and X band can be different significantly. This is a manifestation of resonant effects, i.e., deviations of radar cross sections from the Rayleigh law. Thus in thunderstorm cores of high reflectivities, one should expect an excess of S-band reflectivities over X-band ones.

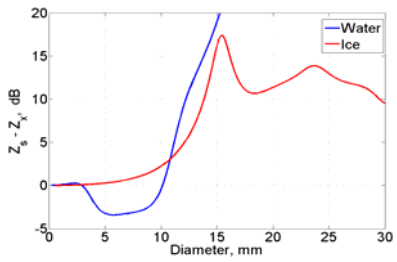

Fig. 7. Reflectivity difference at S and X bands for water drops (blue line) and ice spheres (red line).

In Fig. 8, examples of range profiles of Z and Z_{DR} at both wavelengths are shown. Reflectivity at S band exceeds 60 dBZ which is usually a good indication of hail. In Fig. 8(a,c), measured and corrected Z and Z_{DR} practically coincide thus the correction procedures work poorly: reflectivity deviations beyond 70 km at the two wavelengths are large. Underestimation of attenuation leads also to significant underestimation of differential reflectivity (Fig. 8c). Underestimation of attenuation in hail occurs due to symmetry of tumbling hailstones with respect to horizontally and vertically polarized waves. Due to this symmetry, differential phase from hailstones is about zero which leads to severe underestimation of attenuation based on φ_{dp} measurements.

A different example is shown in Figs. 8(b,d). It is seen that reflectivities at X and S bands are about equal at the boundaries of the strong cell. Thus the correction procedure severely overestimates corrected Z and Z_{DR} at the rear boundary of the cell.

Analyzing ψ and φ_{dp} profiles in zones with reflectivity larger than 60 dBZ at S band we noticed that δ at X band frequently exceeds 10^o. Calculations of the backscatter differential phase for rain show that δ is smaller than 10^o. Phase δ as a function of the rain rate is shown in Fig. 9(a) for Marshall-Palmer drop size distribution. Range profiles of ψ and φ_{dp} at X band are shown in Figs. 9(b,c,d). It is seen that $\delta = \psi - \varphi_{dp}$ can reach 30^o, i.e., a value that is well above the maximum "rain" number. So large δ could be used for hail detection at X band. This is a preliminary conclusion that requires an additional study.

6. Conclusions

Procedures to correct XERES' reflectivity and differential reflectivity for attenuation using the self consistent method with constraints on measured differential phase are applied. Attenuation correction at S band was based on the linear fit between measured differential phase and attenuation. The corrected polarimetric variables are compared against each other. Radar reflectivity Z and differential reflectivity Z_{DR} measured at X and S band are generally consistent in areas with reflectivities less than 45 dBZ. In such cases, the correction procedures work well up to 120 km (Fig. 5). We do not have data for longer distances because XERES, to be collocated with KOUN, sat low on the ground during the experiments.

In cases wherein radar radials contain areas with Zs > 45 dBZ, we frequently see underestimation of Zx and Z_{DRx} which is due to underestimation of attenuation based on measurements of the total differential phase (Figs. 6a,c). Less frequently, we get overestimation of Zx and Z_{DRx}. These malfunctions of the attenuation correction procedures could be due to the presence of ice graupel.

In cases with Zs > 60 dBZ, we usually observe severe underestimation of attenuation at X-band (Figs. 8a,c). This could be due to the presence of hail that do not contribute to the differential phase but severely attenuates X-band radiation. We measured large positive Zs – Zx in reflectivity cores of thunderstorms which can be expected in

the presence of hail and is a result of the resonant effects.

Calculations show that the differential phase upon scattering, δ, at X band in rain remains lower than 10^o at all rain rates. In thunderstorm cores with Zs > 55 dBZ, we measured δ at X-band well above 10^o that is a manifestation of resonant effects. In some cases δ reaches 33^o (Figs. 9b,c,d). Such large δ could be used as an indication of hail.

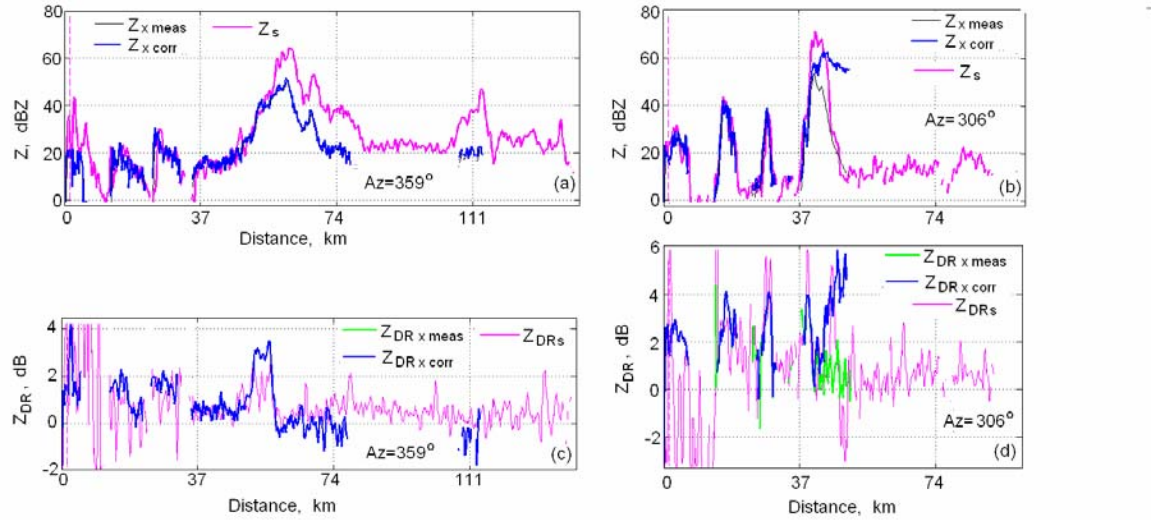

Fig. 8. Same as in Fig. 5 but for different azimuths. In panels (a) and(c) measured and corrected variables at X band practically coincide.

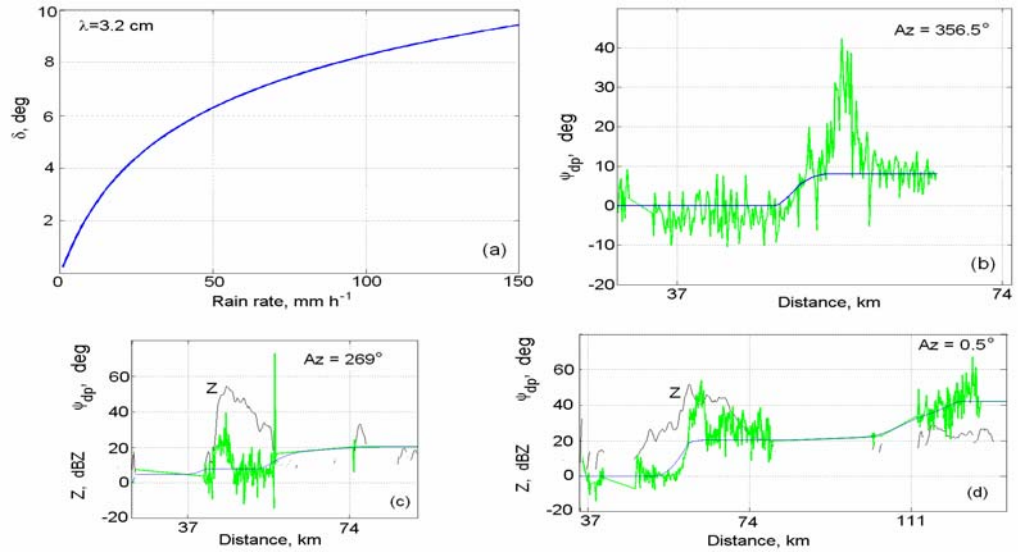

Fig. 9. (a): Backscatter differential phase as function of the rain rate for the Marshall-Palmer drop size distribution. (b,c,d): Range profiles of the measured differential phase at X-band (green lines) and filtered phase (blue lines). El = 1.45^o, 10 February 2009.

References

Alexander, C. R., and J. Wurman, 2005: The 30 May 1998 Spencer, South Dakota, storm. Part I: The structural evolution and environment of the tornadoes. *Mon. Wea. Rev.*, **133,** 72-97.

Anagnostou, E. N., M. N. Anagnostou, W. F. Krajewski, A. Kruger, and B. J. Miriovsky, 2004: High-resolution rainfall estimation from X-band polarimetric radar measurements. *J. Hydrometeor.*, **5,** 110-128.

Anagnostou, E. N., M. N. Anagnostou, J. Vivekanandan, 2006: Correction for rain path specific and differential attenuation of X-band dual-polarization observations. IEEE Trans.**GRS-44**, 2470-2480.

Bluestein, H. B., M. M. French, R. L. Tanamachi, S. Frasier, K. Hardwick, F. Junyent, and A. L. Pazmany, 2007: Close-range observations of tornadoes in supercells made with a dual-polarization, X-band, mobile Doppler radar. *Mon. Wea. Rev.*, **135,** 1522-1543.

Brandes, E.A., G. Zhang, and J. Vivekanandan, 2002: Experiments in rainfall estimation with a polarimetric radar in a subtropical environment. *J. Appl. Meteor*., **41**, 674 – 685.

Bringi, V.N., V. Chandrasekar, N. Balakrishnan, and D.S. Zrnic, 1990: An examination of propagation effects on radar measurements at microwave frequencies. *J. Atmos. Oceanic Technol.*, **7,** 829-840.

Bringi, V. N. and V. Chandrasekar, 2001: *Polarimetric Doppler Weather Radar. Principles and Applications.* Cambridge University Press. 636 pp.

Hitchfield, W., and J. Bordan, 1954: Errors inherent in the radar measurement of rainfall at attenuating wavelengths. *J. Meteorol.,* **11**, 58-67.

Hubbert, J., and V. N. Bringi, 1995: An iterative filtering technique for the analysis of copolar differential phase and dual-frequency radar measurements. *J. Atmos. Oceanic Technol.*, **12,** 643-648.

Iwanami, K., R. Misumi, M. Maki, T. Wakayama, K. Hata, and S. Watanabe, 2001: Development of a multiparameter radar system on mobile platform. Preprints, *30th Conference on Radar Meteorology*, Munich, Germany, Americal Meteorological Society, 104-106.

Marzoug, M., and P. Amayenc, 1991: Improved range –profiling algorithm of rainfall rate from a speceborn radar with path-integrated attenuation constrint. *IEEE Trans*, **GRS-29**, 584-592.

Matrosov, S. Y., D. E. Kingsmill, B.E. Martner, and F.M. Ralph, 2005: The utility of X-band polarimetric radar for quantitative estimates of rainfall parameters. *J. Hydrometeor.,* **6**, 248-262.

Matrosov, S. Y., D. R. Cifelli, P.C. Kennedy, S.W. Nesbitt, S.A. Rutledge, V.N. Bringi, and B.E. Martner. 2006: A comparative study of rainfall retrievals based on specific differential phase shifts at X- and S-band radar frequencies. *J. Atmos. Oceanic Technol.*, **23**, 952-263.

Park, S.G., V.N. Bringi, V. Chandrasekar, M. Maki, and K. Iwanami, 2005: Correction of Radar Reflectivity and Differential Reflectivity for Rain Attenuation at X Band. Part I: Theoretical and Empirical Basis. *J. Atmos. Oceanic Technol.*, **22**, 1621–1632.

Park, S.-G., M. Maki, K. Iwanami, V. N. Bringi, and V. Chandrasekar, 2005: Correction of Radar Reflectivity and Differential Reflectivity for Rain Attenuation at X Band. Part II: Evaluation and Application. *J. Atmos. Oceanic Technol.*, **22,** 1633-1655.

Pazmany, A. L., F. J. Lopez, H. B. Bluestein, and M. Kramar, 2003: Quantitative rain measurements with a mobile, X-band, polarimetric Doppler radar. Preprints, *31st Conference on Radar Meteorology*, Seattle, WA, American Meteorological Society, 858-859.

Snyder, J.C., 2008: Attenuation correction techniques and hydrometeor classification of high-resolution, X-band, dual-polarized mobile radar data of severe convective storms. Master Thesis. Oklahoma University, 148 pp.

Testud, J., E. Le Bouar, E. Obligis, and M. Ali-Mehenni, 2000: The rain profiling algorithm applied to polarimetric weather radar. *J. Atmos. Oceanic Technol.*, **17,** 332-356.

Ulabi, F.T., R.C. Moore, A.K. Fung. 1981: *Microwave remote sensing.* V. 1. Addison-Wesley Publishing, 456 pp.

Yanjiao, X., W. Bin, C. Xiaohui, Y. Xianming, and Z. Qian1, 2008: Data Quality Control of X-Band Polarimetric Doppler Radar on Wheels.